Electronic Supplementary Material (ESI) for Chemical Communications.

Supporting Information

Pt Nanoparticles Supported on Nb-Modified TiO_2 as an Efficient Heterogeneous Catalyst for the Conversion of Cellulose to Light Bioalcohols

Zerui Su,[a] Jian Zhang,*[a] Shiyao Lu[a] and Feng-Shou Xiao*[a,b]

[a.] Beijing Advanced Innovation Center for Soft Matter, Science and Engineering, Beijing University of Chemical Technology, Beijing 100029, China. Email: jianzhangbuct@mail.buct.edu.cn

[b.] Key Lab of Biomass Chemical Engineering of Ministry of Education, College of Chemical and Biological Engineering, Zhejiang University, Hangzhou 310027, China. E-mail: fsxiao@zju.edu.cn (F.-S. Xiao)

EXPERIMRNTAL SECTION

Catalyst preparation

Ethanol (AR), silica (SiO_2, AR), and alumina (Al_2O_3, AR) were purchased from Aladdin Chemical Co., Ltd. Anatase (TiO_2, AR) and cellulose (50μm, AR) were bought from Sigma-Aldrich Co., Ltd. Niobium(V) ethoxide (99.999% metals basis) and glycolaldehyde were obtained from Alfa Aesar Chemical Co., Ltd. Chloroplatinic acid (H_2PtCl_6, 37.5% metals basis), glucose (AR), 5-hydroxymethylfurfural (5-HMF, AR), sorbitol (AR), hydrochloric acid (HCl, 36%), nitric acid (HNO_3, 65%), and sufuric acid (H_2SO_4, 98%) were purchased from Sino-Pharm Chemical Reagent Co., Ltd. Magnisium oxide (MgO, AR) was purchased from Adamas Chemical Co., Ltd.

Synthesis of Pt nanoparticles supported on Nb-modified TiO_2 (Pt/NbTi-x). The Nb-modified TiO_2 was firstly synthesized by the procedures in the following: desired amount of niobium ethoxide was dissolved into 1.25 g of ethanol (trace of water in ethanol was removed by refluxing the mixture of magnsium powder and ethanol for 2 h), followed by adding 1 g of anatase into the solution. The obtained mixture was ground in a mortar under ambient conditions until all the ethanol was evaporated. The obtained solid was allowed to age at room temperature for 2 days. The Nb-modified TiO_2 support (designated as NbTi-x, where x represents the feeding molar ratio of Nb/Ti for the catalyst) was obtained by treatments at 300 °C in air (relative humidity ~30%) for 2 h. Nb-modified TiO_2 loaded Pt nanoparticles was synthesized by incipient wetness impregnation method. Chloroplatinic acid aqueous solution was applied as the Pt precursor. After removing water at 80 °C and reducing the solid at 300 °C for 4 h in H_2, the samples designated as H_2-treated Pt/NbTi-x (where x represents the molar Nb/Ti in the catalyst) were obtained. The catalysts were passivated in flowing 0.5% O_2/N_2 for 1 h at room temperature after reduction. To adjust catalytic performance, the Pt/NbTi catalyst was also pretreated in air (relative humidity ~30%) at 150 °C for 1 h (designated as air-treated Pt/NbTi catalyst).

Synthesis of Nb_2O_5 loaded Pt nanoparticles (Pt/Nb_2O_5). The Pt/Nb_2O_5 sample was synthesized through similar procedures of the Pt/NbTi-x samples except that the

Nb_2O_5 support was obtained by aging niobium ethoxide at room temperature for 2 days and calcining the solid at 300 °C in the air (relative humidity ~30%) for 2 h.

Synthesis of SiO_2, Al_2O_3, TiO_2 (anatase), and MgO loaded Pt nanoparticles (Pt/ SiO_2, Pt/Al_2O_3, Pt/TiO_2, and Pt/MgO). The SiO_2, Al_2O_3, TiO_2 (anatase), and MgO supported Pt nanoparticles were synthesized through impregnation method: the support was impregnated with chloroplatinic acid aqueous solution and aging at room temperature for 8 h. Then, the mixture was heated at 60 °C to evaporate water, the Pt/ SiO_2, Pt/Al_2O_3, Pt/TiO_2, and Pt/MgO were obtained by reducing the solid at 300 °C for 2 h in H_2.

Catalytic tests. The conversion of cellulose to bioalcohols were performed on a high-pressure autoclave equipped with a quartz bottle. As a typical run, 200 mg of cellulose and 100 mg of catalyst were mixed in 20 ml of H_2O. The autoclave was purged with H_2 for five times and then charged with 3 Mpa of H_2. The autoclave was heated to desired temperature 220 °C (the temperature was mesured by a thermometer inside the autoclave) and reacted for 8 h. After reaction, the autoclave was tansferred into an ice bath to stop the reaction. The products were separated by filtration and anlyzed by a LC-10AT liquid chromotography equipped with a RID detector and a Shimadzu GC-17A gas chromotography equipped with a FID detector. As the alkane products (C_1~C_6) yields were lower than 0.2% under all reaction conditions detected, which are not shown in the maintext.

Recyclable tests. The recyclability of the catalysts were studied by separating the catalyst after reaction, washing with H_2O, ethanol, and ethyl acetate, drying under 80 °C, heating at 150 °C in static air (relative humidity ~30%) for 1 h, and used for the next run. and then using in the next run. After used for 7 times, the used catalyst was calcined at 500 °C for 1 h to remove the coke species. The calcined catalyst was reduced at 300 °C in H_2 for 1 h and heated at 150 °C in static air (relative humidity ~30%) for 1 h before the next run.

Catalyst Characterization

X-ray diffraction (XRD) patterns were collected on a Rigaku D/MAX 2550 diffractometer with Cu Kα radiation (λ=1.5418 Å). Pt and Nb loading amounts were

determined by inductively coupled plasma (ICP) analysis (Perkin-Elmer 3300DV). The samples were tested by procedures in the following: the as-dried samples were mixed with newly made aqua regia (V_{HCl}/V_{HNO3} = 3/1) in a PTFE bottle, heating at 150 °C for 8 h to solve the Pt and Nb species (caution: the treatment process should be performed within a hood because aqua regia is corrosive and toxic). Afterwards, H_2SO_4 was slowly added into the above mixture to dissolve the Ti species, followed by diluting the solution with de-ionized water. After reaction, a trace amount of Nb and Ti species in the reaction solution was determined by Angilent ICP-MS 7900. The organic compounds in the solution were removed by rotary evaporation before tests. Transmission electron microscopy (TEM) and scanning transmission electron microscopy (STEM) images were performed on a JEM-2100F electron microscopy (JEOL, Japan) with an acceleration voltage of 200 kV. As the Pt nanoparticles in the Pt/NbTi catalysts were encapsulated in an oxide sheath, it is demanding to clearly evaluate the Pt dispersion by TEM analysis, the dispersions of Pt nanoparticles were determined on a HUASI DAS-7200 chemsorption instrument equipped with a thermal conductivity detector (TCD). The samples were firstly pretreated at 300 °C in flowing H_2 for 1 h and subsequent cooled to 50 °C. After sweeping the samples at 50 °C for 1 h, the samples were pulse treated with flowing CO/He at 50 °C until saturation adsorption. The Pt dispersion was calculated by the adsorption amount/Pt loading amount with the assumption that CO was qualitatively adsorbed on the surface of Pt nanoparticles. Raman spectra were recorded on a Renishaw in Via-Reflexm equipped with a laser (532 nm). The samples were pretreated in N_2 at 300 °C for 1 h before tests. Temperature-programmed-desorption of NH_3 (NH_3-TPD) were carried out on a BELCAT-B chemisorption instrument equipped with a thermal conductivity detector (TCD). The samples were firstly pretreated at 400 °C in flowing He for 1 h and subsequent adsorption of NH_3 at 50 °C. After sweeping the samples at 50 °C for 2 h, the samples were heated to 550 °C with a ramp rate of 10 °C/min. CO-adsorption IR spectra were recorded using a VERTEX 70 BRUKER spectrometer equipped with ZnSe window, MCT/A detector, and high temperature reaction chamber. Before CO adsorption, the samples were pretreated in flowing He (30

mL/min) at 300 °C for 1 h, then cooled to room temperature. During the redox treatment of the catalysts, 10% H_2/He (30 mL/min) and air (30 mL/min) were applied in the experiments. The background spectrum was collected in He at room temperature. Afterwards, the flowing gas was switched to 1% CO/He, the CO-adsorption IR spectra were recorded until the absorbances were steady. Pyridine adsorption FT-IR spectra were performed on a Bruker Tensor 27 FT-IR spectrometer. The samples were pretreated at 300 °C for 1 h, adsorption of pyridine at 50 °C, and vacuum treated at 150 °C for each test. XPS (X-ray photoelectron spectroscopy) spectra were obtained on a Thermo Fisher Scientific ESCALAB 250Xi photoelectron spectroscopy system using an Al Kα (1486.6 eV) X-ray source. The binding energy (BE) values were calibrated using the C1s peak at 284.8 eV.

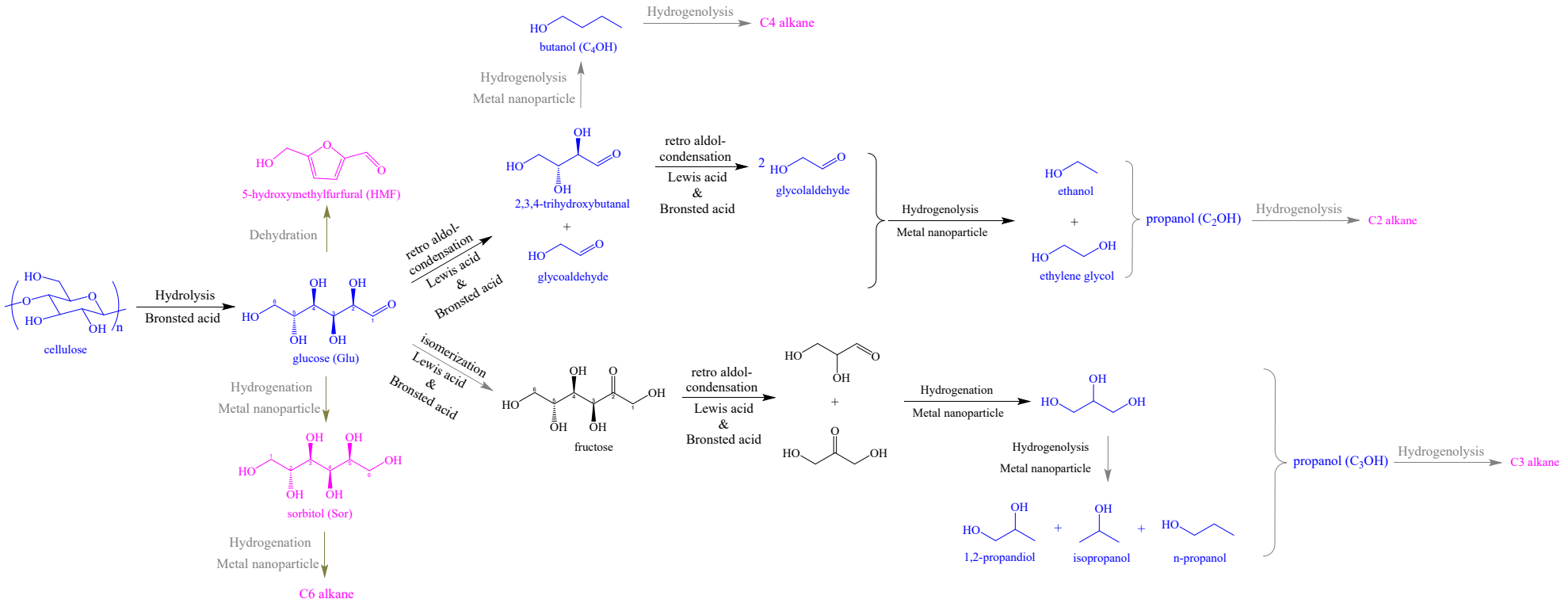

Scheme S1. The reaction process in the conversion of cellulose to ethanol.

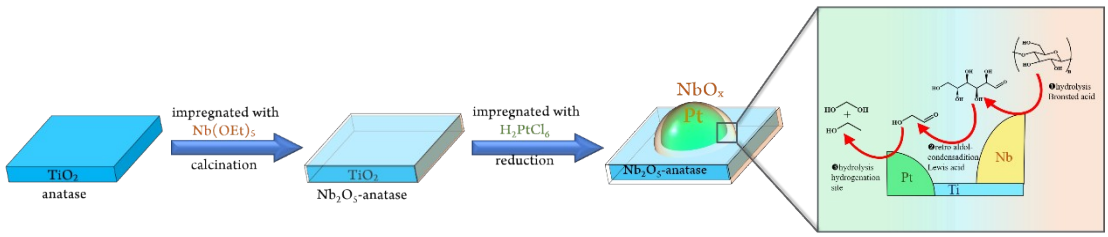

Scheme S2. The synthesis process of the Pt/NbTi catalyst.

Note: Based on STEM images and elemental analysis results (Figures 2 and S7), we propsed that the Pt/NbTi catalyst contains the structure in the following: the Pt nanopaticle was surrounded by an amorphous NbO_x sheath, which were supported on mixed oxide support (Scheme S2 and inset in Figure 2b). This structure renders the formation of adjacent Pt, Nb and Ti sites (Scheme S2), which is helpful for tandem reactions of hydrolysis of cellulose to glucose, sequential retro aldol-condensation of glucose to glycolaldehyde, and hydrogenation of glycolaldehyde to bioethanol, the important steps for conversion of cellulose into bioalcohols.

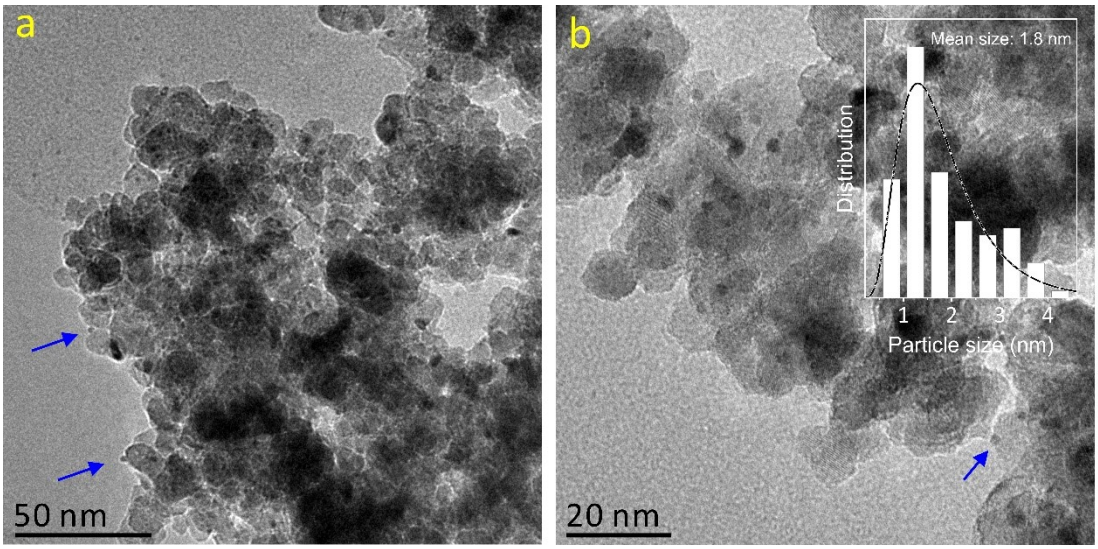

Figure S1. (a and b) TEM images of the Pt/TiO_2 sample. Inset in b: Pt nanoparticle size distribution of the Pt/TiO_2 sample. The blue arrows in a and b highlight the bare Pt nanoparticles.

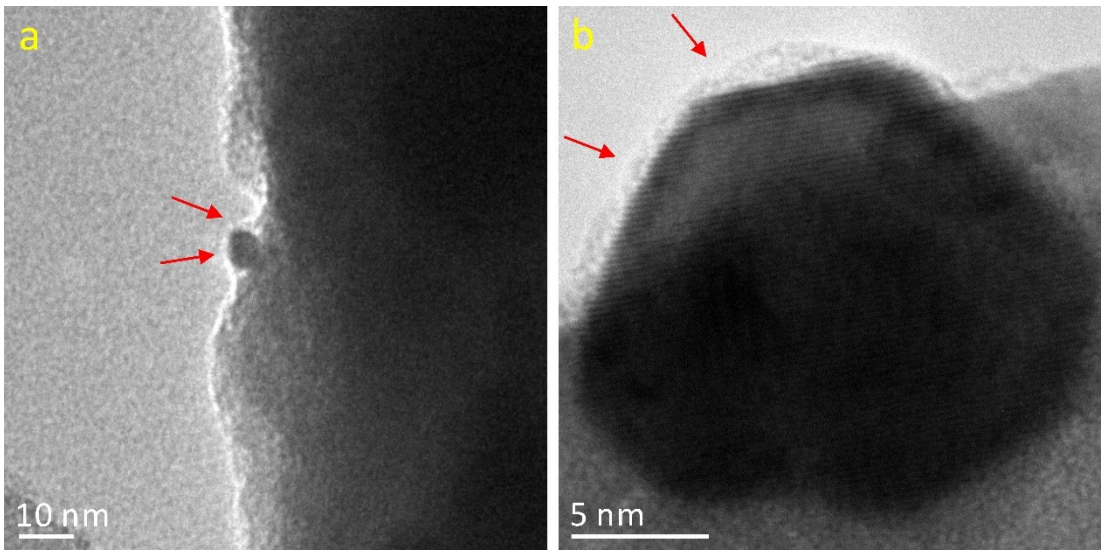

Figure S2. (a and b) HR-TEM images of the Pt/Nb_2O_5 sample. The red arrows in a and b highlight the oxide layer on the Pt nanoparticles.

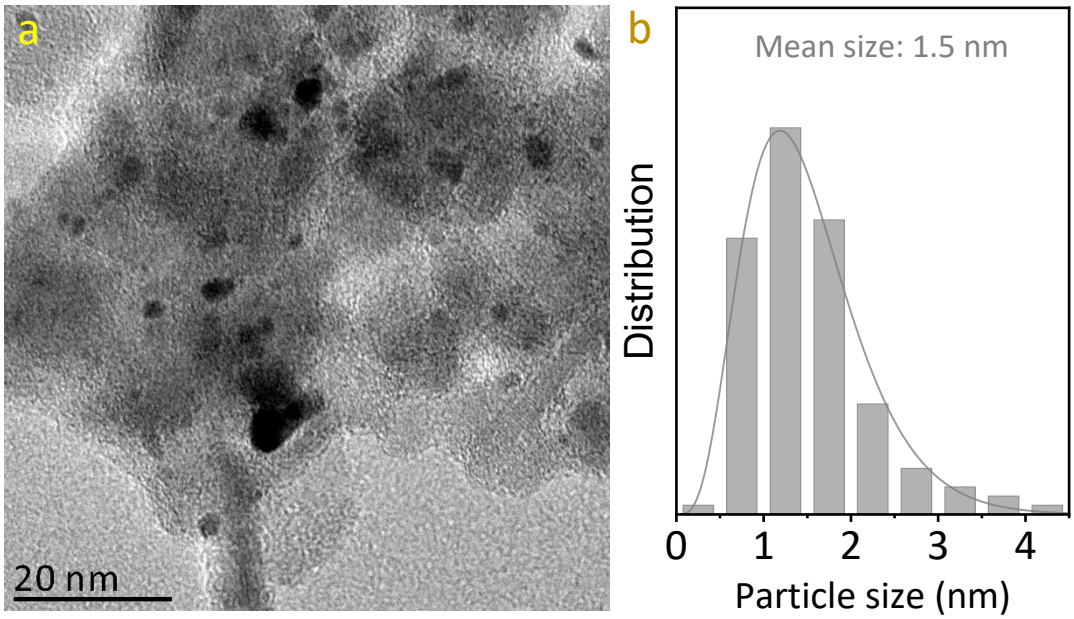

Figure S3. (a) TEM image and (b) Pt nanoparticle size distribution of the Pt/Al_2O_3 sample.

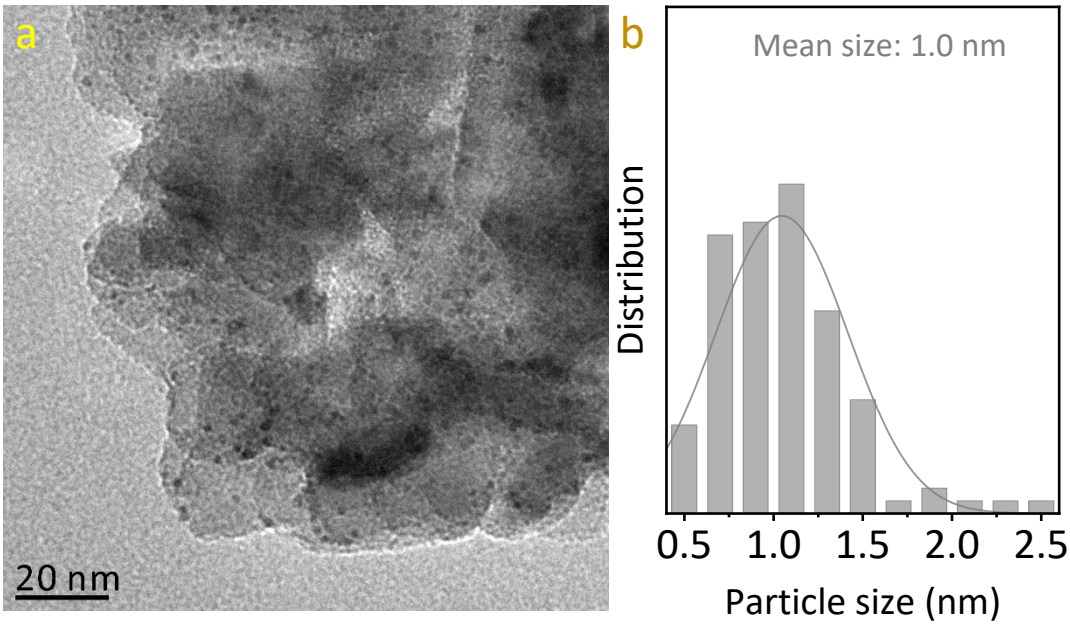

Figure S4. (a) TEM image and (b) Pt nanoparticle size distribution of the Pt/MgO sample.

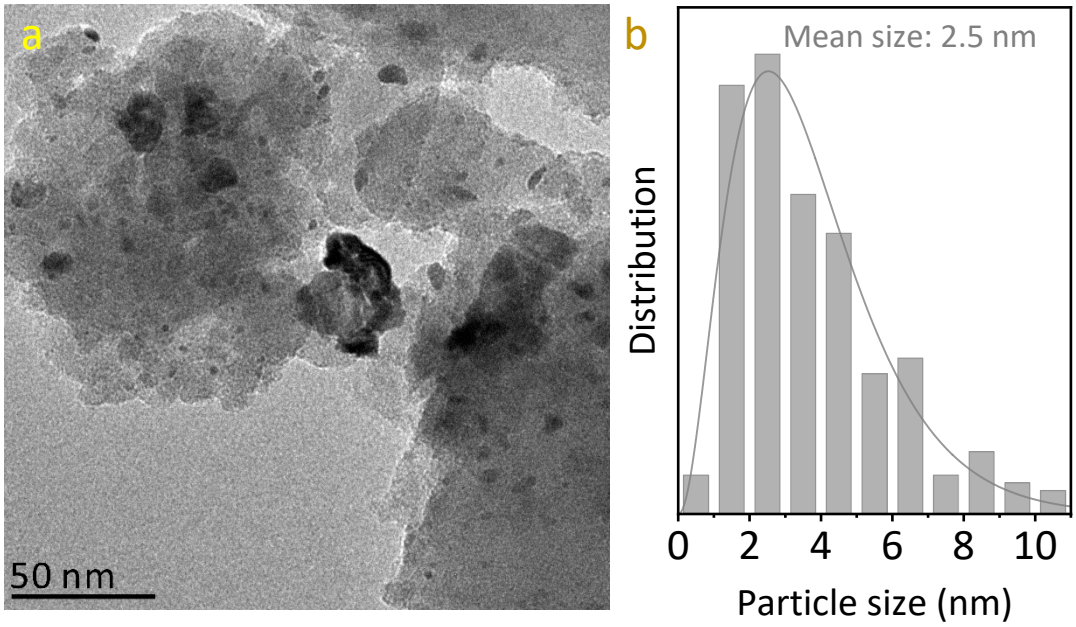

Figure S5. (a) TEM image and (b) Pt nanoparticle size distribution of the Pt/SiO_2 sample.

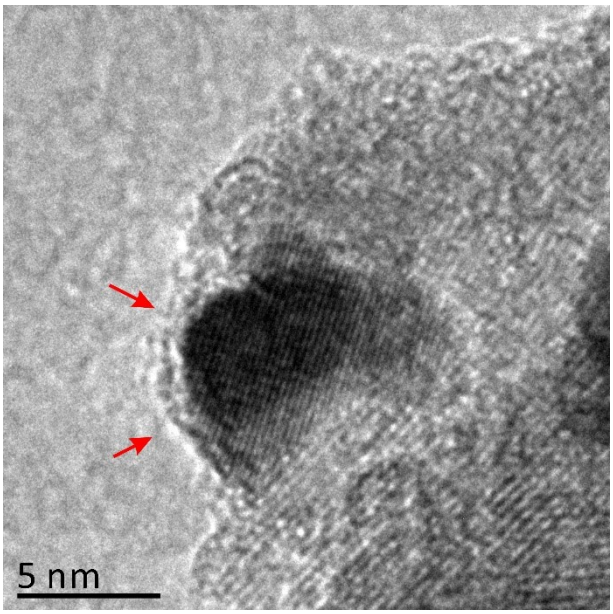

Figure S6. HR-TEM image of the H_2-treated Pt/NbTi-0.05 sample.

Note: As the Pt nanoparticles in the Pt/NbTi catalysts were encapsulated in an oxide sheath, it is demanding to clearly evaluate the Pt dispersion by TEM analysis. The Pt dispersions were characterized by CO chemisorption (Table S3).

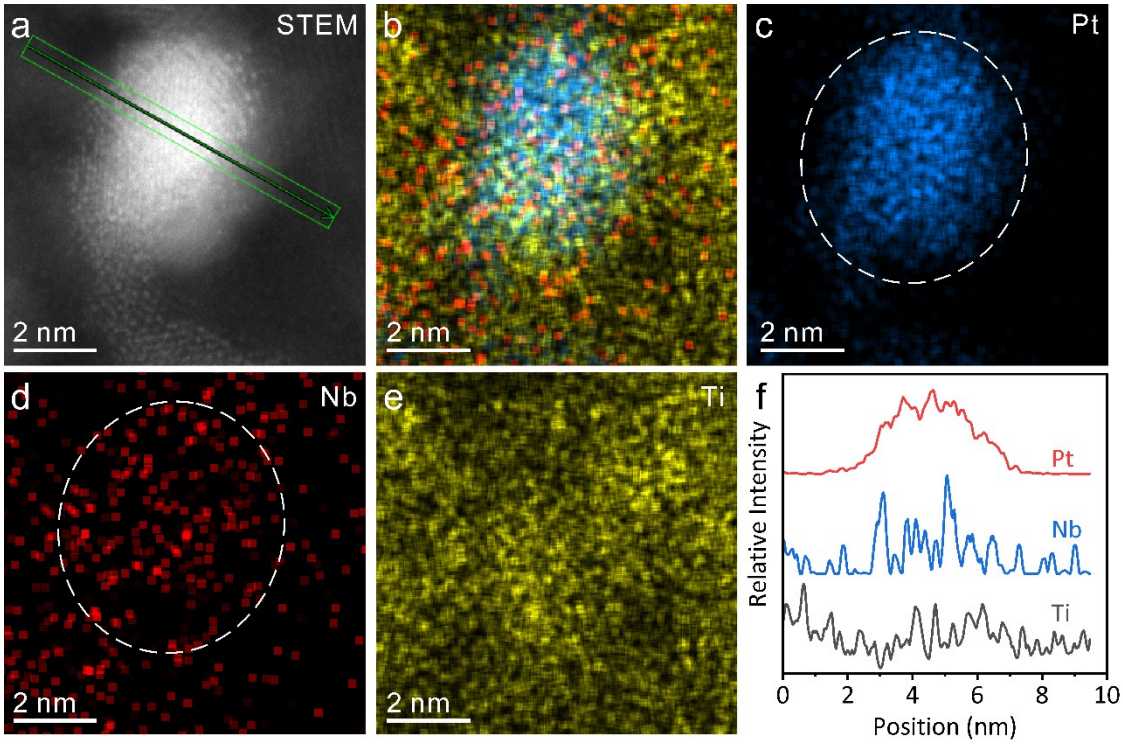

Figure S7. (a) HAADF-STEM, and corresponding (b) elemental, (c) Pt, (d) Nb, (e) Ti mappings, and (f) line scan data of the air-treated Pt/NbTi-0.05 catalyst. The line can data in f corresponded to the red arrow in a. The white dashed circle highlighted the enrichment of Nb species on Pt nanoparticles.

Note: To confirm the enrichment of the Nb species around Pt nanoparticle, the Pt, Nb, and Ti elemental maps were obtained (Figure S7b-e). Notably, it can be observed that the Nb species (Figure S7d) were enriched around the Pt nanoparticle (Figure S7c), indicating that the amorphous oxide sheath around the Pt nanoparticle is Nb-containing species. Furthermore, we have also displayed line scan around the Pt nanoparticles (Figure S7f). Interestingly, it can be observed that the signals of Nb species corresponded to those of the Pt species, while the Ti species did not. This phenomenon also confirmed that the amorphous oxide sheath around the Pt nanoparticle is Nb-containing species but not Ti-containing species.

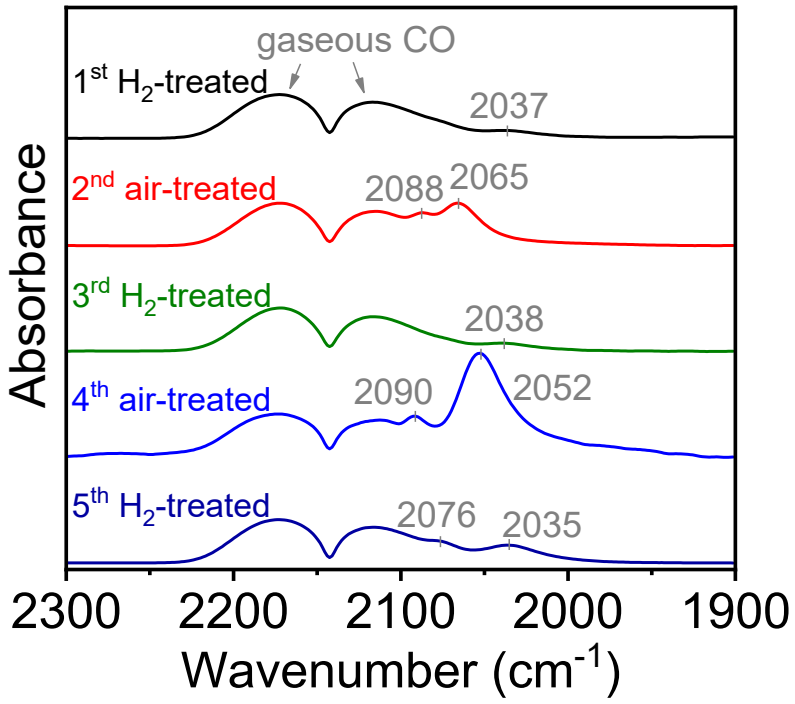

Figure S8. CO-adsorption FT-IR spectra of the Pt/NbTi-0.05 sample after treatments in the following: 1st as-obtained H_2-treated catalyst, 2nd treated in a humid air at 150 °C for 1 h, 3rd treated in H_2 at 300 °C for 1 h, 4th treated in a humid air at 150 °C for 1 h, and 5th treated in H_2 at 300 °C for 1 h (relative humidity in the air at 30%). The first line in the range of 2050 – 1950 cm^{-1} was enlarged for convenience of observation.

Note: CO-adsorption FT-IR spectra were obtained to support the presence of SMSI in the Pt/NbTi catalysts (Figure S8). The as-obtained H_2-treated Pt/NbTi-0.05 catalyst exhibited bands at 2170, 2110, and 2037 cm^{-1}, which are associated with gaseous CO and CO adsorbed on negatively charged Pt species (Figure S8). Based on STEM images and elemental analysis results, we proposed that the Pt/NbTi catalyst contains the structure in the following: the Pt nanopaticle was surrounded by an amorphous NbO_x sheath, which were supported on mixed oxide support (Sheme S2 and inset in Figure 2). The presence of negatively charged Pt species indicates the elentron transfer between the Pt nanoparticles and the NbO_x sheath, whcih is a typical feature of SMSI.

The 2nd air-treatment of the H_2-reduced Pt/NbTi catalyst led to the shift of the peak at 2025 cm^{-1} to 2088 and 2065 cm^{-1}. Typically, the Pt species contain CO-adsorption IR bands with higher wavenumbers possessed more positively charge. Therefore, the blue shift of the CO bands on the 2nd air-treatment FT-IR spectra was caused by the partial oxidation of the Pt species during the air-treatment.

During the redox teatment of the SMSI induced Pt/NbTi catalyst, the NbO_x sheath would be reversely strengthened and weakened by the reduction and oxidation treatments (Figure S9). However, the oxide sheath is not densely enough to totally block the CO-adsorption sites. Therefore, the Pt/NbTi catalyst exhibited peak at ~2035 cm^{-1} in 3rd H_2-treated and 5th H_2-treated spectra, and the absorbance of these peaks are much weaker than those on the air-treated conditions. In the 4th air-treated spectrum, it can be clearly observed two peaks at 2090 and 2052 cm^{-1}, which should be attributed to the metallic and negatively charged Pt species. In the subsequential 5th H_2-treated spectrum, these two peaks was shifted to 2076 and 2035 cm^{-1}, both of which should be associated with the negatively charged Pt species.

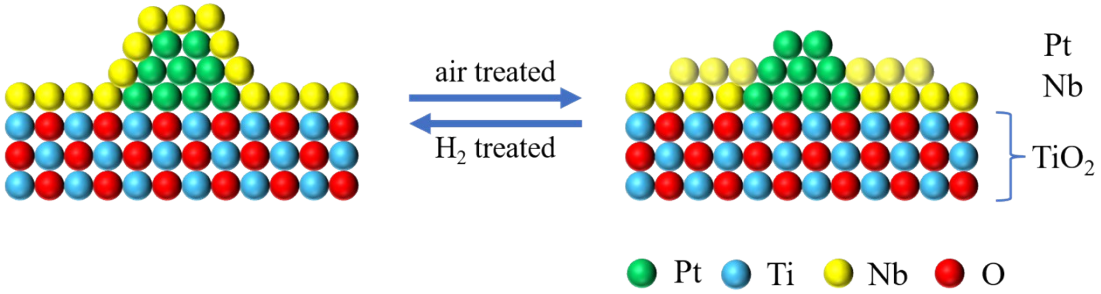

Figure S9. Model representing the variation of NbO_x oxide sheath on the Pt/NbTi catalyst during the redox treatment.

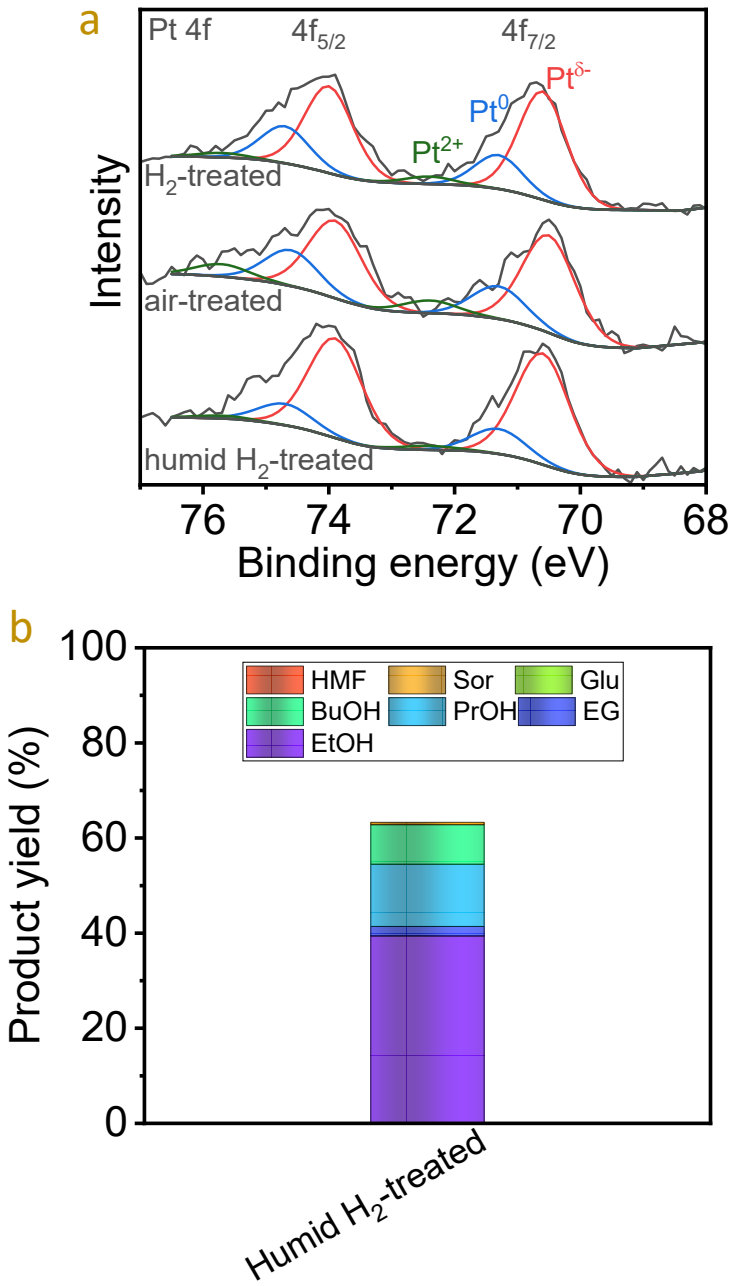

Figure S10. (a) Pt 4f XPS spectra of the dry H_2-treated, air-treated, and humid H_2-treated (30% relative humidity) Pt/NbTi-0.05 catalyst; (b) Catalytic conversion of cellulose over the dry H_2-treated, air-treated, and humid H_2-treated (30% relative humidity) Pt/NbTi-0.05 catalysts. EtOH, EG, PrOH, BuOH, Glu, and Sor denoted as ethanol, ethylene glycol, propanol, butanol, glucose, and sorbitol, respectively.

Note: The Pt 4f XPS spectra of the dry H_2-treated Pt/NbTi-0.05 catalysts are shown in Figure S10a. The H_2-treated Pt/NbTi-0.05 catalyst exhibited Pt $4f_{7/2}$ signals at 70.6,

71.3, and 72.4 eV, which should be related to the $Pt^{\delta-}$, Pt^0, and Pt^{2+} species, respectively.[1,2] Correspondingly, the relative amount of the $Pt^{\delta-}$, Pt^0, and Pt^{2+} species are 72.4%, 22.5%, and 5.1% (Table S2), showing that the Pt nanoparticles are electron-rich.

We have also detected the Pt 4f XPS spectra of the humid air-treated Pt/NbTi-0.05 catalyst (Figure S10a). The Pt/NbTi-0.05 catalyst also exhibited three peaks associated with the $Pt^{\delta-}$, Pt^0, and Pt^{2+} species. The relative amount of the $Pt^{\delta-}$, Pt^0, and Pt^{2+} species in the humid air-treated Pt/NbTi-0.05 catalyst are 68.0%, 23.2%, and 8.8% (Table S2). Relative higher amount of Pt^0, and Pt^{2+} species in the humid air-treated Pt/NbTi-0.05 catalyst indicates that the Pt species are slightly oxidized during the treatment of catalyst in the humid air.

We have proved that the different treat conditions of the catalysts greatly influenced the acidic amounts in the Pt/NbTi-0.05 catalyst, which significantly affect the catalytic performances. The influence of the valence of Pt on the catalytic performance should also be studied. Therefore, we have also treated the Pt/NbTi-0.05 catalyst with humid H_2 (30% relative humidity) to obtain different Pt valence state with the humid air-treated Pt/NbTi-0.05 catalyst. XPS spectra confirm that the Pt valence state in the humid H_2-treated Pt/NbTi-0.05 catalyst is similar to that of the dry H_2-treated Pt/NbTi-0.05 catalyst (Table S2), which is relatively lower than that of the humid air-treated Pt/NbTi-0.05 catalyst (Table S2). Interestingly, the humid H_2-treated Pt/NbTi-0.05 catalyst exhibited comparable total light bioalcohols yield (62.8%) and ethanol yield (39.4%) to those of the humid air-treated Pt/NbTi-0.05 catalyst (Figure S10b), indicating that the valence of Pt almost did not affect the catalytic performance.

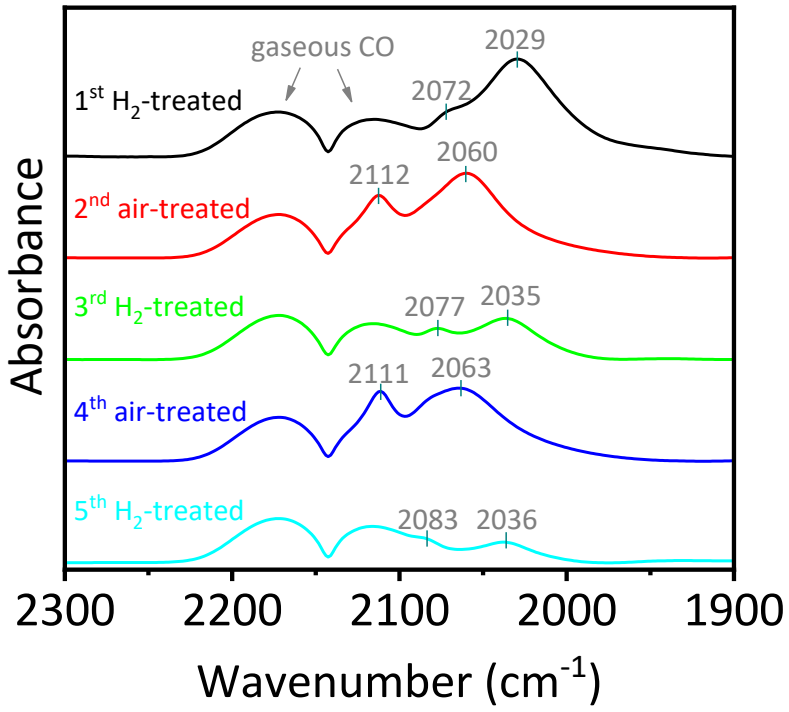

Figure S11. CO-adsorption FT-IR spectra of the Pt/TiO_2 sample after the following sequential treatments: 1st treated in H_2 at 300 °C for 1 h, 2nd treated at 150 °C for 1 h, 3rd treated in H_2 at 300 °C for 1 h, 4th treated at 150 °C for 1 h, and 5th treated in H_2 at 300 °C for 1 h.

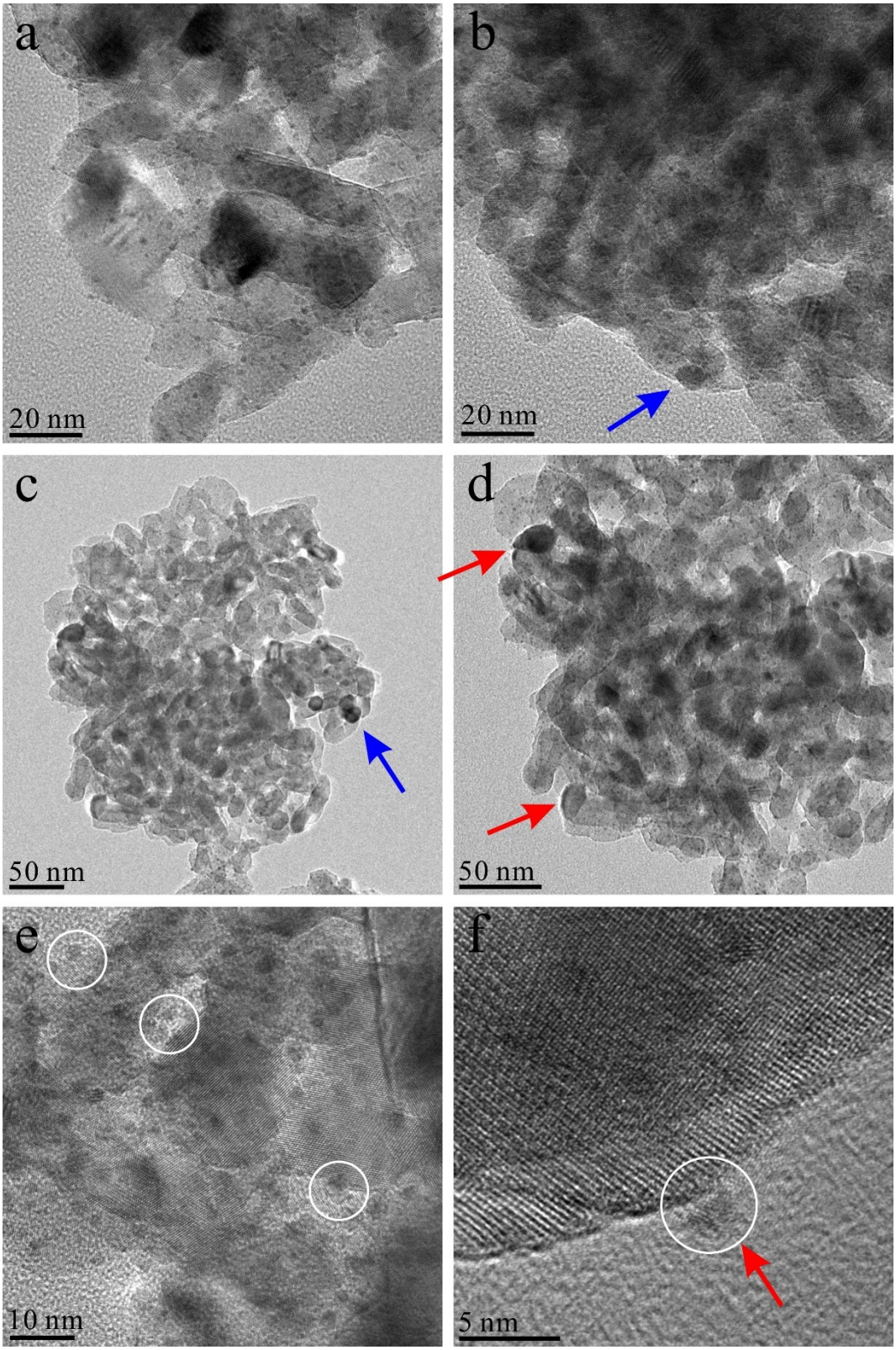

Figure S12. TEM images of the Pt/TiO_2 catalyst reduced at (a and b) 400, (c and d) 500, and (e and f) 600 °C. The red and blue arrows highlighted the encapsulated and naked Pt nanoparticles, respectively.

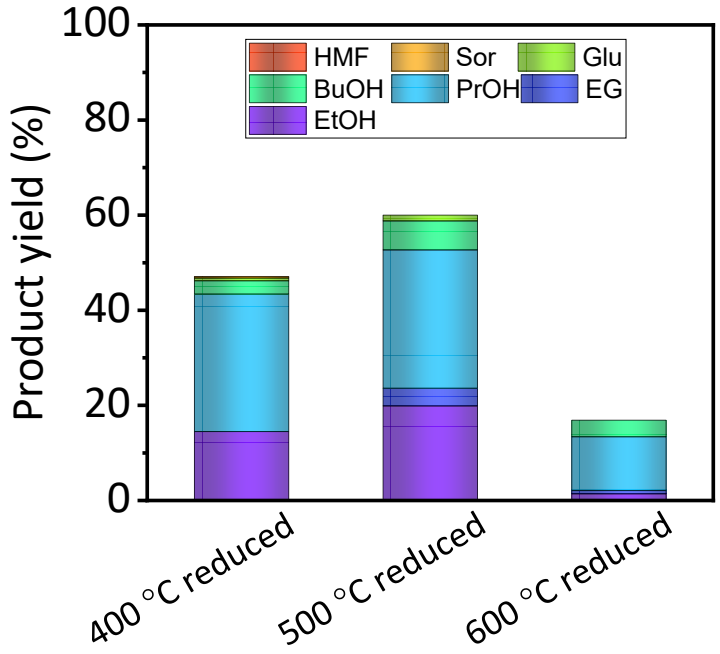

Figure S13. Catalytic conversion of cellulose over the Pt/TiO_2 catalysts reduced at 400~600 °C. EtOH, EG, PrOH, BuOH, Glu, and Sor denoted as ethanol, ethylene glycol, propanol, butanol, glucose, and sorbitol, respectively.

Note: Pt/TiO_2 is a classic example of SMSI effect where TiO_x layer is formed on Pt nanoparticles under H_2 reduction. However, high reduction temperature (typically >400 °C) is essential for the construction of SMSI in the Pt/TiO_2. During the synthesis of Pt/NbTi-0.05 catalyst, the reduction temperature was only at 300 °C, which could not construct TiO_x sheath around the Pt nanoparticle. We have also elevated reduction temperature to 400~600 °C to examine whether there is SMSI on Pt/TiO_2. As shown in Figure S12, the Pt/TiO_2 catalyst reduced at 400 °C did not exhibit obvious encapsulated Pt nanoparticles (Figure S12a) even though a little amount of the Pt nanoparticles were sintered (Figure S12b). The Pt/TiO_2 catalyst reduced at 500 °C still exhibited partially sintered Pt nanoparticles (Figure S12c), and it can be observed some encapsulated Pt nanoparticles on the TEM image (Figure S12d), indicating that high reduction temperature is beneficial for the induction of SMSI in the Pt/TiO_2 catalyst. Notably, the Pt/TiO_2 catalyst reduced at 600 °C exhibited obvious encapsulated Pt nanoparticles (Figure S12e and f), which is in accordance

with the results reported previously. The catalytic performances of the Pt/TiO_2 catalyst reduced at 400~600 °C were also studied (Figure S13). However, the light alcohol yield and ethanol yield over these catalysts were lower than those of the Pt/NbTi-0.05 catalyst, which might be caused by the lack of Brønsted acid sites in the Pt/TiO_2 catalyst.

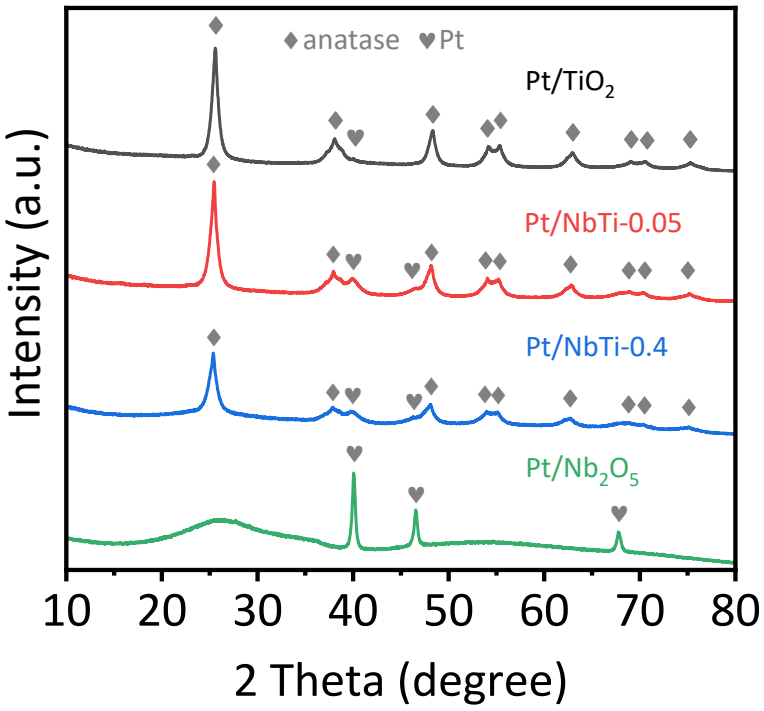

Figure S14. XRD patterns of the Pt/TiO_2, Pt/NbTi-0.05, Pt/NbTi-0.4, and Pt/Nb_2O_5 samples.

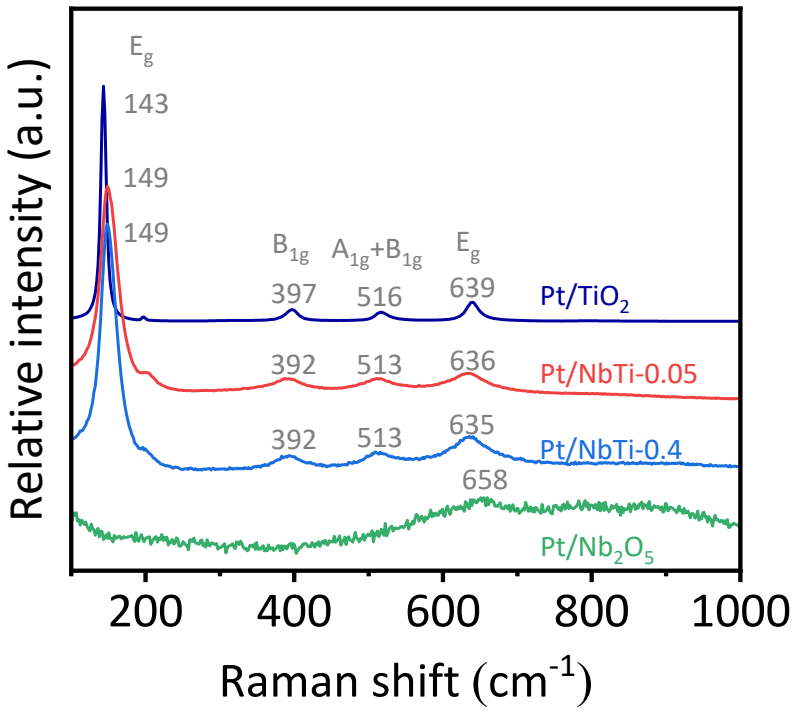

Figure S15. Raman spectra of the Pt/TiO_2, Pt/NbTi-0.05, Pt/NbTi-0.4, and Pt/Nb_2O_5 samples.

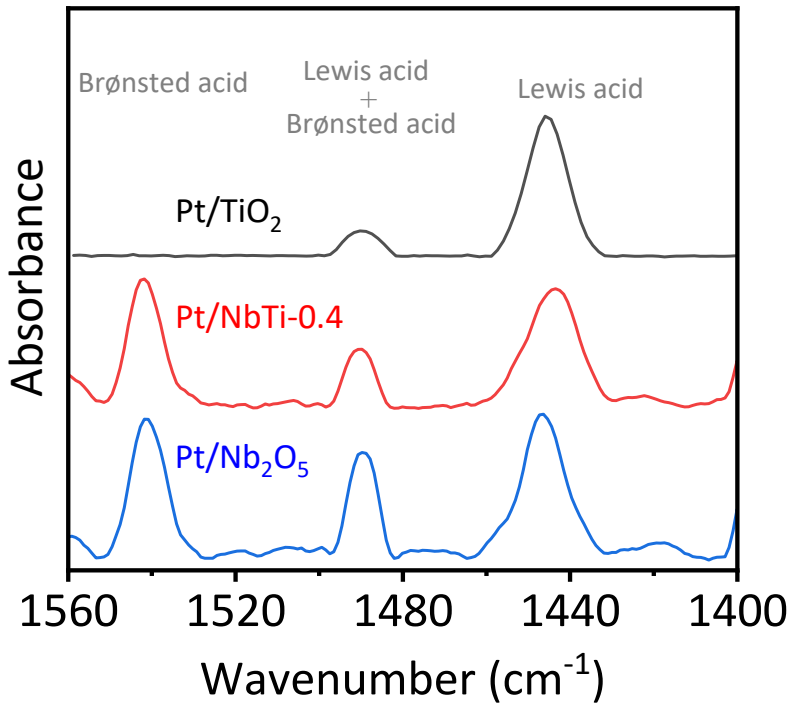

Figure S16. Pyridine-adsorption FT-IR spectra of the Pt/TiO_2, Pt/NbTi-0.4, and Pt/Nb_2O_5 samples.

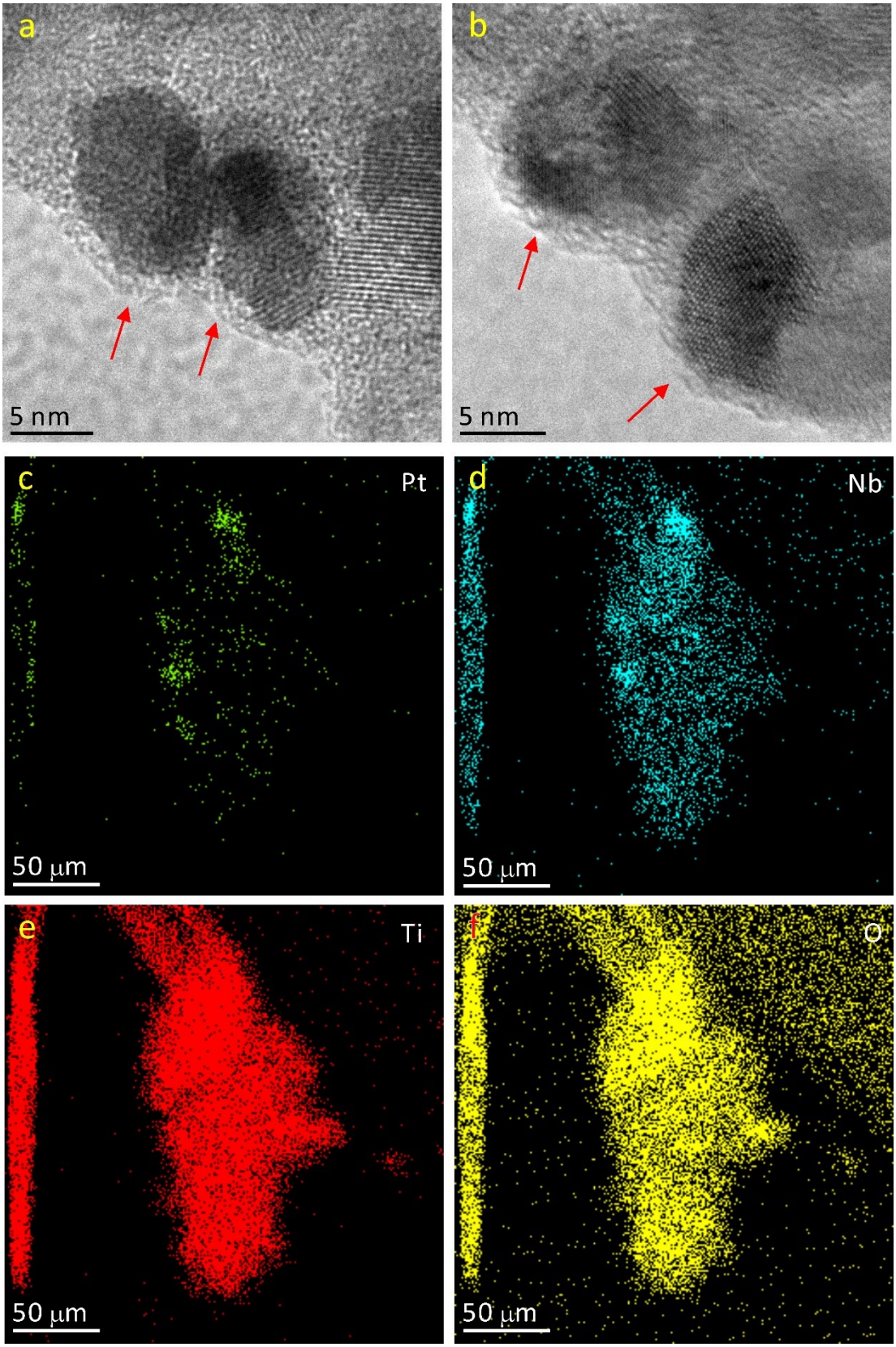

Figure S17. (a and b) HR-TEM images and (c) Pt, (d) Nb, (e) Ti, and (f) O elemental map of the Pt/NbTi-0.4 sample. The red arrows in a and b highlight the oxide layer on the Pt nanoparticles.

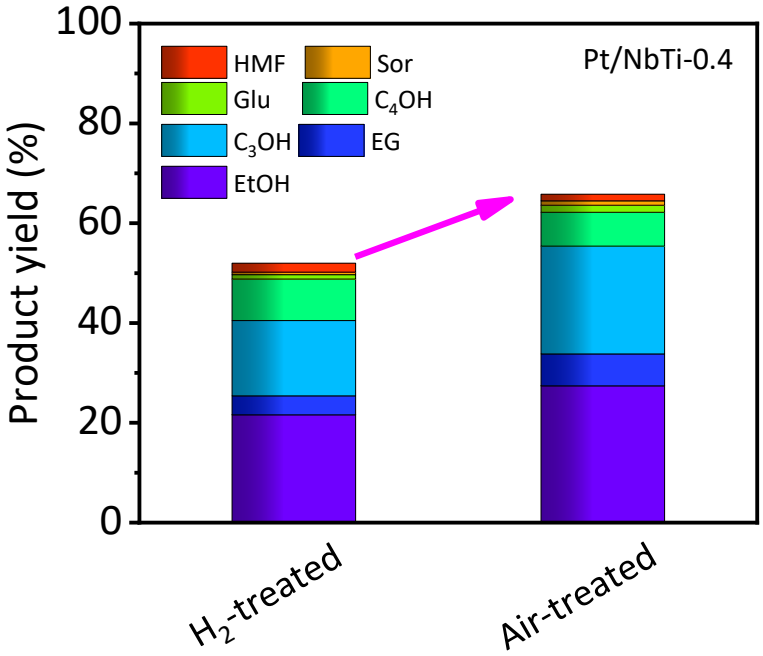

Figure S18. Catalytic conversion of cellulose to ethanol over H_2-treated and air-treated Pt/NbTi-0.4 catalysts. EtOH, EG, PrOH, BuOH, Glu, and Sor denote ethanol, ethylene glycol, propanol, butanol, glucose, and sorbitol, respectively. Reaction conditions: 0.3 g of cellulose, 0.15 g of catalyst, 30 mL of H_2O, 220 °C, 3 MPa of H_2 at room temperature, 8 h. The air-treated catalyst was treated the as-synthesized catalyst in air (relative humidity ~30%) at 150 °C for 1 h.

Note: The air-treated Pt/NbTi catalysts with changing Nb loadings also exhibited good catalytic performances. For example, the H_2-treated Pt/NbTi catalysts with Nb loading at 17.3% (designated as Pt/NbTi-0.4, Figure S17) showed yield of light bioalcohols at 48.8%, while the air-treated Pt/NbTi-0.4 catalyst exhibited the yield of 62.2% (Figure S18). NH_3-TPD results also confirm the enhanced acidic concentration in the Pt/NbTi-0.4 catalyst (Figure S19) in the pretreatment with a humid air.

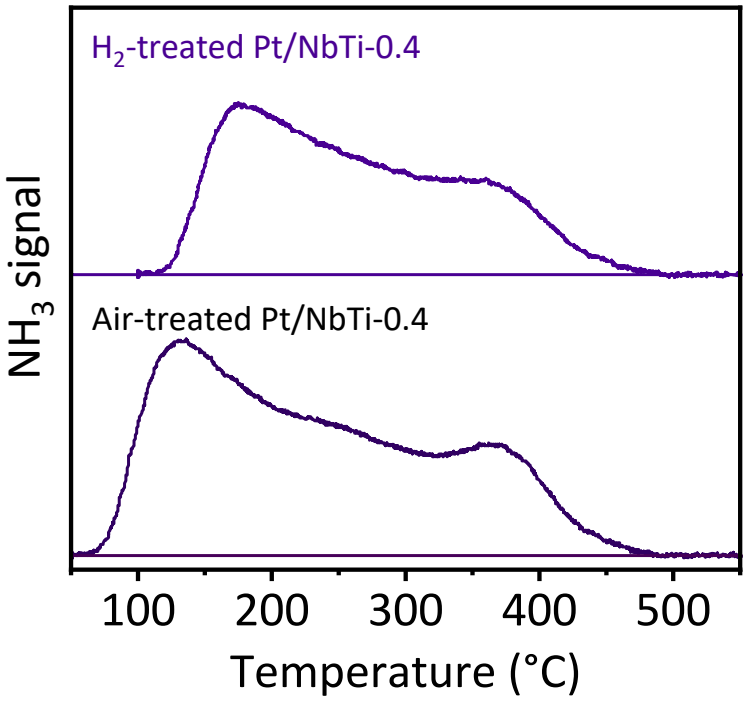

Figure S19. Temperature-programmed-desorption of ammonia (NH_3-TPD) profile of the H_2-treated and air-treated Pt/NbTi-0.4 samples.

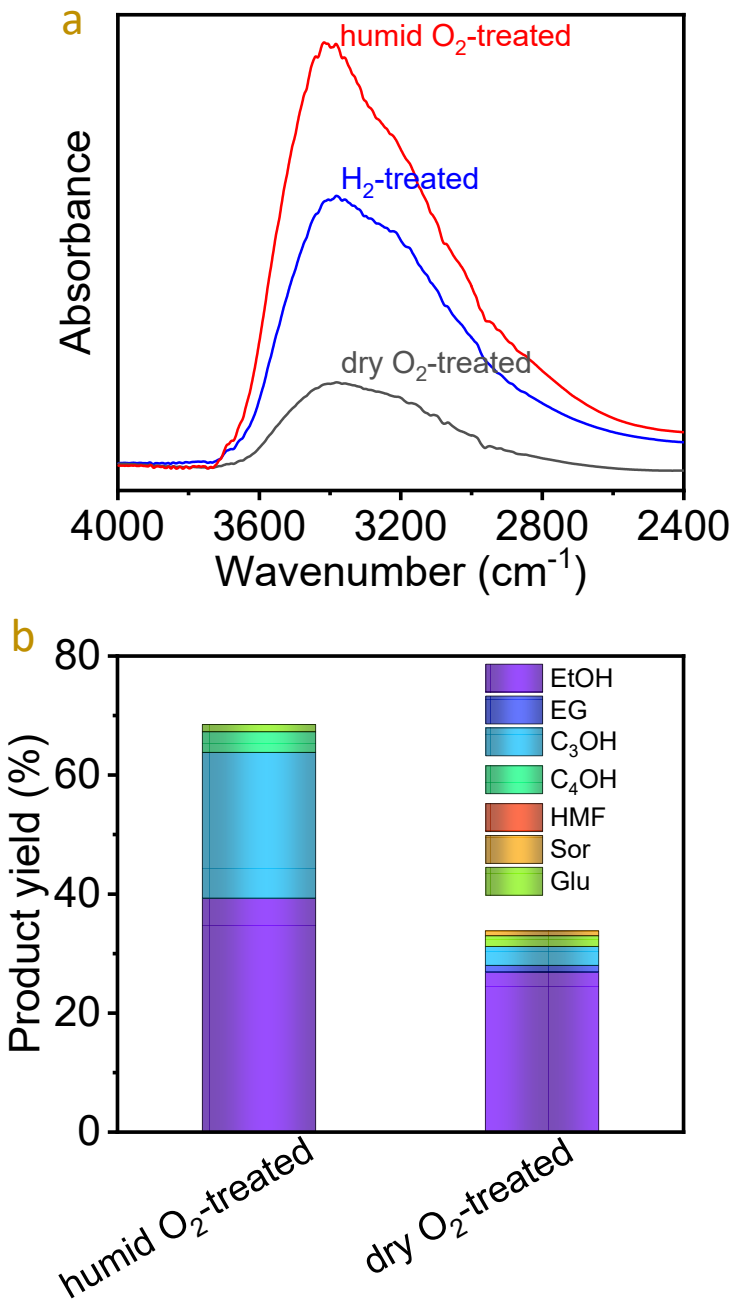

Figure S20. (a) FT-IR spectra of the H_2-treated and O_2-treated Pt/NbTi-0.05 samples; (b) Catalytic conversion of cellulose over the Pt/NbTi-0.05 catalyst pretreated in flowing O_2 with and without H_2O (3% H_2O / 97% O_2). EtOH, EG, PrOH, BuOH, Glu, and Sor denoted as ethanol, ethylene glycol, propanol, butanol, glucose, and sorbitol, respectively. Reaction conditions: 0.3 g of cellulose, 0.15 g of catalyst, 30 mL of H_2O, 220 °C, 3 MPa of H_2 at room temperature, 8 h.

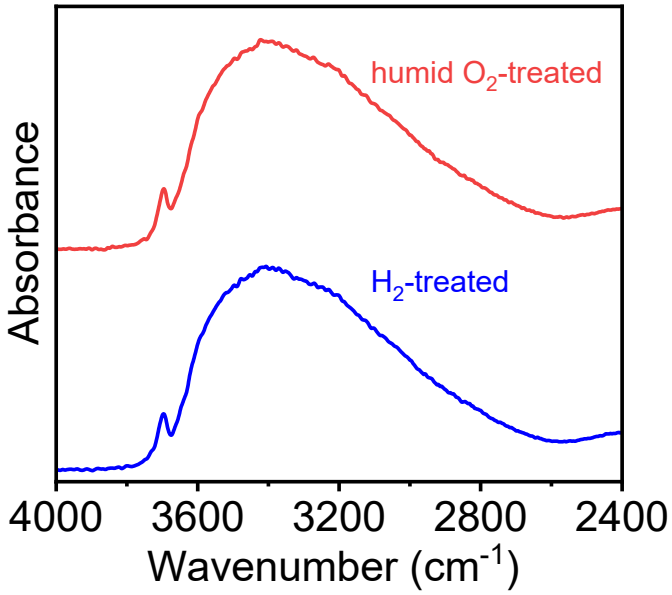

Figure S21. FT-IR spectra of the H_2-treated and humid O_2-treated Pt/TiO_2 samples. Reaction conditions: 0.3 g of cellulose, 0.15 g of catalyst, 30 mL of H_2O, 220 °C, 3 MPa of H_2 at room temperature, 8 h.

Note: The effect of hydroxyl groups on the surface of TiO_2 on the catalytic performance should be studied. To study the variation of the surface hydroxyl groups on the Pt/TiO_2 catalyst, *in situ* FT-IR spectra of the H_2-treated and air-treated Pt/TiO_2 samples (Figure S21) were recorded. The Pt/TiO_2 catalysts pretreated under different conditions exhibited broad peak between 3630-2800 cm^{-1}, which should be associated with the hydroxyl species (Figure S21). Notably, the peak absorbances of the hydroxyl species on the H_2-treated and air-treated Pt/TiO_2 samples are similar, indicating that the hydroxyl groups on the Pt/TiO_2 catalyst were not largely affected by the pretreatments. Furthermore, the H_2-treated and air-treated Pt/TiO_2 catalysts have very similar yields of light alcohols at 27.8 and 28.7 % (Figure 1a). These results evidenced that surface hydroxyl groups of TiO_2 were not affected by the pretreatments, which could not influence the catalytic performance of Pt/TiO_2 catalyst in the conversion of cellulose into light bioalcohols.

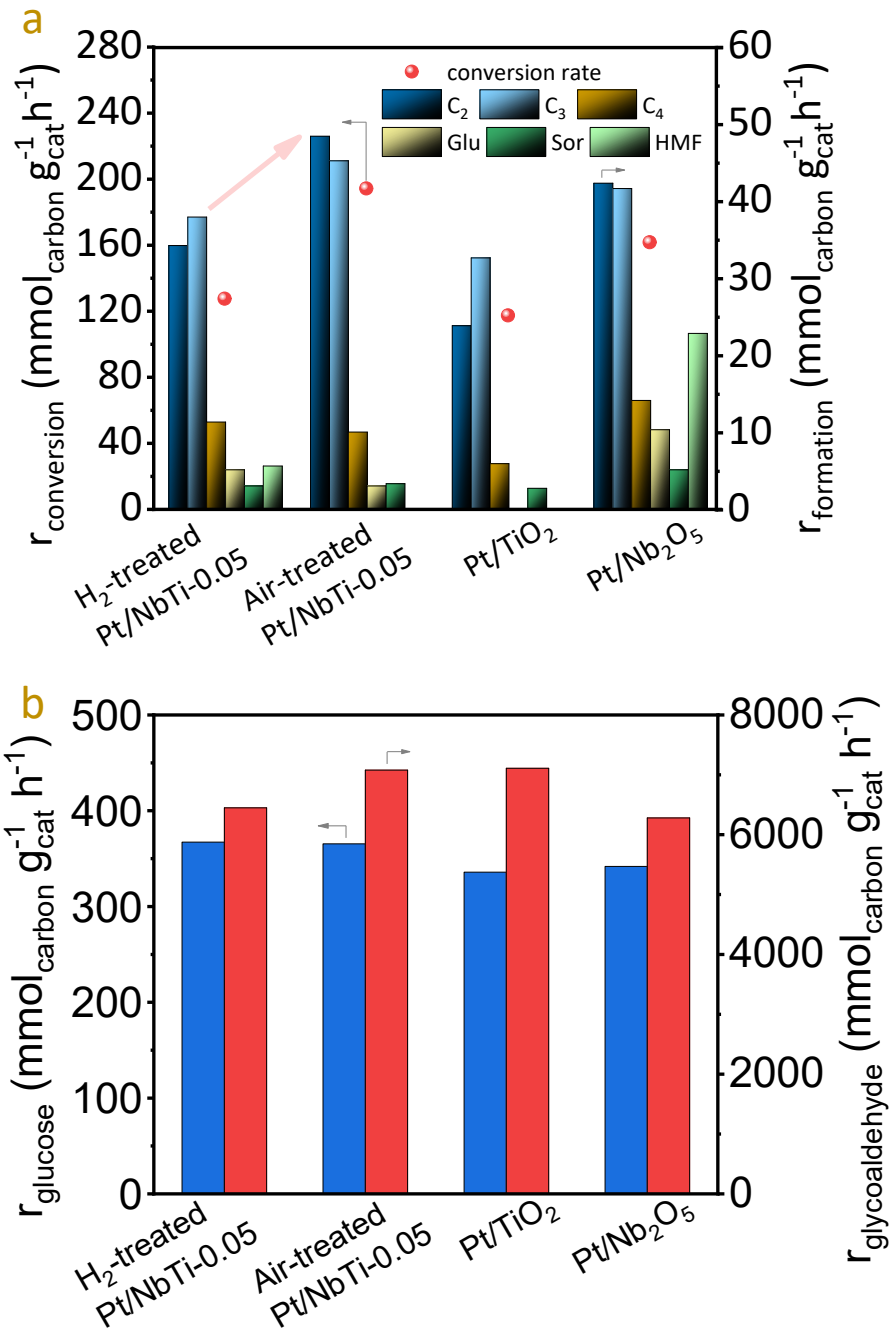

Figure S22. (a) Kinetic data in the catalytic conversion of (a) cellulose and (b) glucose and glycolaldehyde over the Pt/NbTi-0.05, Pt/TiO_2, and Pt/Nb_2O_5 catalysts. C_2, C_3, C_4, Glu, Sor, and HMF denoted as ethanol and ethylene glycol, propanol, butanol, glucose, sorbitol, and 5-hydroxymethylfurfural, respectively.

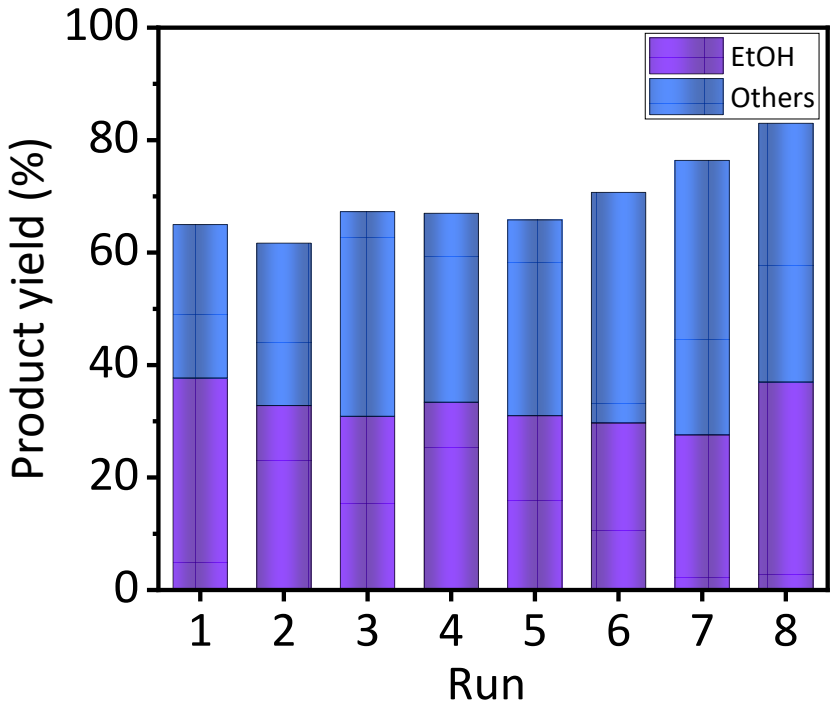

Figure S23. Recyclable tests in the catalytic conversion of cellulose to ethanol over Pt/NbTi-0.05 catalyst. EtOH denotes ethanol, others contain ethylene glycol, propanol, butanol, glucose, and sorbitol. After 7 runs the catalyst was treated in air (relative humidity ~30%) at 150 °C for 1 h to remove the coke on the catalyst.

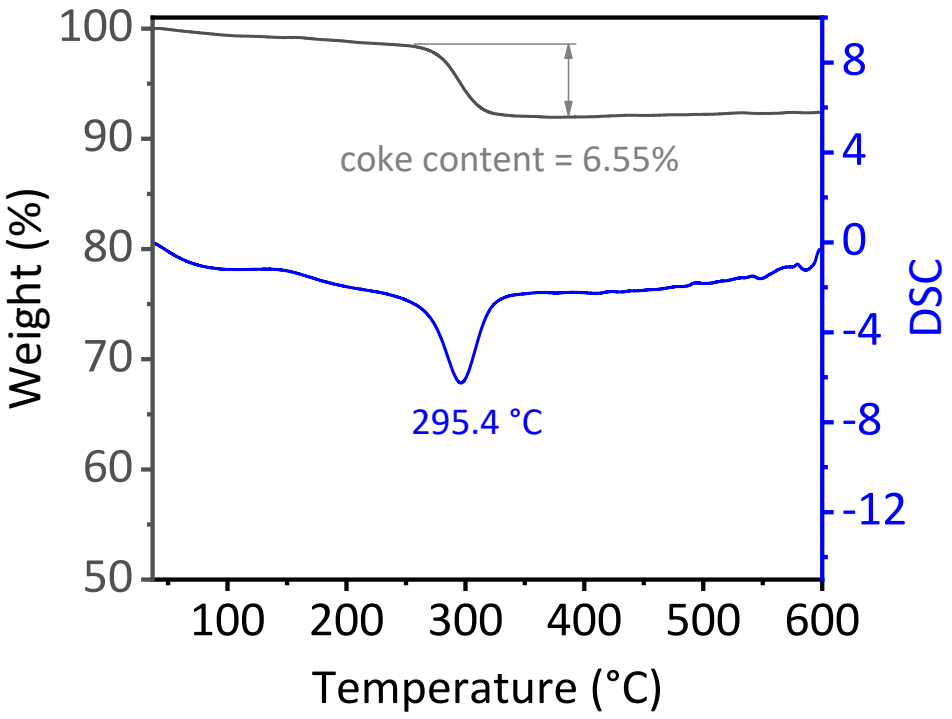

Figure S24. Thermal gravity (TG) curve of the used Pt/NbTi-0.05 sample.

Table S1 Total light alcohol and ethanol yields at suitable reaction conditions over the Pt/NbTi-0.05 and previous reported catalysts.

Catalyst	Catalyst amount (g)	Cellulose amount (g)	Reaction conditions			ETOH yield (%)	Light alcohol yield (%)	Ref.
			T (°C)	Time (h)	P_{H_2} (MPa)			
Ni@C+H_3PO_4	0.15	0.4	200	3	5.5	69.1	85.2	3
H_2WO_4+Pt/ZrO_2	0.05+0.1	0.2	250	5	4	32.0	64.8	4
Mo/Pt/WO_x	0.1	0.15	245	2	6	43.2	60.8	5
Ru-WO_x/HZSM-5 + Ru-WO_x	0.1+0.1	0.1	235	20	3	87.5	87.5	6
$CuMgAlO_x$	0.1	0.1	300	4	-	-	48.8	7
Pt/WOx + Pt@HZSM-5 Hol	0.2	0.2	245	4	4	54.4	61.8	8
Pd-Cu-WO_x/SiO_2	0.2	1	300	10	4	42.5	76.9	9
Pt/NbTi-0.05	0.15	0.3	220	8	3	37.7	64.5	This work

Note: Our Pt/NbTi-0.05 catalyst exhibited 64.5% total light alcohol yield and 37.7% ethanol yield at 220 °C. As shown in Table S1, Ni@C catalyst mixed with liquid phosphorous acid (H_3PO_4) are efficient for production of ethanol by cellulose hydrogenolysis, exhibiting total light alcohol and ethanol yield at 85.2% and 69.1%, respectively. However, the use of corrosive H_3PO_4 acid strongly hinders the wide applications of this

system. The W-containing heterogeneous catalysts are very active for conversion of cellulose to bioalcohols, exhibiting total light alcohol and ethanol yield at 60.8-87.5% and 32.0-87.5%, respectively. However, high reaction temperature (235-300 °C) is needed for the conversion of cellulose (Table S1). Furthermore, leaching of W from the catalysts might be an obstacle for recycling these catalysts.

Table S2 The concentration of the $Pt^{\delta-}$, Pt^0, and Pt^{2+} species on the Pt/NbTi-0.05 catalyst characterized by XPS spectra.

Treat conditions	$Pt^{\delta-}$ (70.6 eV)	Pt^0 (71.3 eV)	Pt^{2+} (72.4 eV)
Pretreated in dry H_2 at 300 °C for 2 h	72.4%[a]	22.5%[a]	5.1%[a]
Pretreated in humid at 150 °C for 1 h	68.0%[a]	23.2%[a]	8.8%[a]
Pretreated in humid H_2 at 150 °C for 1 h	78.7%[a]	18.1%[a]	3.2%[a]

[a] calculated from the data for XPS measurements

Table S3. Metal loading amount and acid concentrations of various catalysts.

Entry	Catalyst	Metal loading amount (*wt*%)[a]		Pt dispersion (%)[b]	Acid concentration (μmol/g)[c]			B/L[d]
		Pt	Nb		Weak	Medium strong	Total	
1	Pt/NbTi-0.05	4.5	5.1	5.6	226[e]	197[e]	423[e]	0.19
					422[f]	393[f]	815[f]	
2	Pt/NbTi-0.4	4.6	17.3	8.6	336[e]	171[e]	507[e]	0.19
					509[f]	195[f]	704[f]	
3	Pt/TiO_2	4.7	-[g]	18.8	223	316	539	0
4	Pt/Nb_2O_5	4.1	-[h]	4.7	-[h]	-[h]	-[h]	0.41
5	Pt/SiO_2	3.1	-[g]	3.1	-[g]	-[g]	-[g]	-[g]
6	Pt/Al_2O_3	4.0	-[g]	20.1	-[h]	-[h]	-[h]	-[h]
7	Pt/MgO	3.9	-[g]	21.4	-[h]	-[h]	-[h]	-[h]

[a] determined by ICP

[b] determined by CO chemisorption

[c] determined by NH_3-TPD

[d] determined by pyridine-adsorption FT-IR spectra

[e] pretreated in H_2 at 300 °C for 1 h

[f] pretreated in O_2 at 150 °C for 1 h

[g] trace or undetectable

[h] did not detect because of technique reason

References

1 Q. Wang, Y. Li, A. Serrano-Lotina, W. Han, R. Portela, R. Wang, M. A. Bañares and K. L. Yeung, *J. Am. Chem. Soc.*, 2021, **143**, 196-205.

2 G. Zhang, D. Yang and E. Sacher, *J. Phys. Chem. C* 2007, **111**, 565-570.

3 Q. Y. Liu, H. Y. Wang, H. S. Xin, C. G. Wang, L. Yan, Y. X. Wang, Q. Zhang, X. H. Zhang, Y. Xu, G. W. Huber and L. L. Ma, ChemSusChem, 2019, 12, 3977-3987.

4 H. Y. Song, P. Wang, S. Li, W. P. Deng, Y. Y. Li, Q. H. Zhang and Y. Wang, Chem. Comm., 2019, 55, 4304-4306.

5 M. Yang, H. F. Qi, L. Fei, Y. J. Ren, X. L. Pan, L. L. Zhang, X. Y. Liu, H. Wang, J. F. Pang, M. Y. Zheng, A. Q. Wang and T. Zhang, Joule, 2019, 3, 1937-1948.

6 C. Li, G. Xu, C. Wang, L. Ma, Y. Qiao, Y. Zhang and Y. Fu, Green Chem., 2019, 21, 2234-2239.

7 P. H. Galebach, D. J. McClelland, N. M. Eagan, A. M. Wittrig, J. S. Buchanan, J. A. Dumesic and G. W. Huber, ACS Sustain. Chem. Eng., 2018, 6, 4330-4344.

8 Y. Wu, C. Dong, H. Wang, J. Peng, Y. Li, C. Samart and M. Ding, ACS Sustainable Chem. Eng., 2022, 10, 2802-2810.

9 D. W. Chu, Z. C. Luo, Y. Y. Xin, C. Z. Jiang, S. F. Gao, Z. H. Wang and C. Zhao, Fuel, 2022, 292, 120311.